# EVALUATION OF WALL SHEAR STRESS DISTRIBUTION IN UPWARD VERTICAL SLUG FLOW

**Jonathan Sant'Anna Garcez Nobrega, jonathan@fem.unicamp.br**
**Eugênio Spanó Rosa, erosa@fem.unicamp.br**
Faculty of Mechanical Engineering - State University of Campinas, Rua Mendeleyev 200, 13083-860, Campinas, SP, Brazil

***Abstract.*** *It has been shown in the literature that the transport of crude petroleum rich in $CO_2$ under slug flow regime enhances the corrosion process. The present corrosion models take into account several electrochemical factors and to represent the ions mass transfer near the pipe wall they employ the average wall shear stress or even the pressure drop. The models cannot be generalized to all slug flow in field application. In fact, they show a good agreement if applied to field conditions similar to the database where they were developed. In general, these models have a tendency to underestimate the corrosion rate. The causes that lead to the models' under prediction are still unknown but one of the factors may be the use of an average wall shear stress. Indeed, the wall shear stress is not uniform but changes continuously due the passage of the liquid slug followed by the liquid film. The objective of this work is to estimate the local wall shear stress distribution of a gas-liquid mixture flowing upwards in a vertical pipe under slug pattern. The analyses are carried out in a slug unit (a liquid slug trailed by Taylor bubble) for tubes with 50, 75 and 100 mm ID and superficial mixture velocity varying from 1, 2 and 3 m/s. In order to estimate the wall shear stress distribution in the liquid slug and in the liquid film surrounding the Taylor bubble are used, respectively, an axis-symmetric CFD analysis and the one-dimensional liquid film model proposed by Taitel and Barnea (1990). The numerical estimates display two critical points with null wall shear stress along a slug unit. One locates at the liquid film just downstream the Taylor bubble nose and the second at the liquid slug just downstream the Taylor bubble tail. These critical points are used as flags signalizing the regions with positive and negative shear. Near the critical points, the wall shear stress is ever changing. To observe a constant wall shear stress it takes a pipe length of nearly 16 pipe diameters upstream of the liquid slug critical point and approximately 60 pipe diameters downstream the liquid film critical point.*

***Keywords****: two-phase flow, vertical slug flow, wall shear stress, corrosion*

## 1. INTRODUCTION

The slug flow pattern is an intermittent flow due the quasi-periodic occurrence of liquid slugs trailed by elongated gas bubbles. It has been studied since 60's if one considers the works of Nicklin et al. (1962), Moissis and Griffith (1962) and Wallis (1969). The researches concerning this type of flow regime have been motivated by its occurrence in petroleum and nuclear industries.

This work is motivated by a phenomenon encountered in crude oil production lines operating under slug flow, the corrosion rate enhancement. The continuous monitoring and maintenance of pipelines disclosed an under predicted corrosion rate, CR, which has motivated investigations of the slug flow parameters capable to be related to the high CR.

Pioneering works started during nineties relating slug flow influence on corrosion caused by $CO_2$, known as sweet corrosion, due the high occurrence of this contaminant during hydrocarbons production (Green et al., 1990; Sun and Jepson, 1992; Zhou, 1993; Kanwar, 1994; Gopal et al., 1995; Jepson et al., 1996). The authors evidenced that the high level of turbulence present in slug flow has a great impact on CR.

From modelling approach, the wall shear stress, $\tau_w$, was found to be an effective parameter to incorporate the flow influence on corrosion rate. This concept was first introduced by Efird et al. (1993), which studied the flow-accelerated corrosion in a horizontal full pipe liquid flow, developing a CR model, Eq. (1):

$$CR = A \cdot \tau_w{}^n \tag{1}$$

The usage of $\tau_w$ in Eq. (1) is based on the Chilton-Colburn analogy to infer the mass transfer coefficient, k, which ultimately leads to the estimated corrosion rate. The constants A and n are functions of the specific environment and solution chemistry.

For horizontal flow, the use of wall shear stress was replaced by the flow pressure drop equation,

$$\Delta P = 4\tau_w \frac{L}{D}, \tag{2}$$

because the latter is directly proportional to $\tau_w$ and easily measured. In Eq. (2) D is the pipe diameter and L is the axial pipe length where the pressure drop is measured.

It is necessary to emphasize that estimating CR employing $\tau_w$ does not imply the existence of corrosion enhancement by a shear mechanism. There is still a divergence in the literature whether the wall shear stress is able or not, to remove mechanically the corrosion product acting, which acts as a protective coating, usually $FeCO_3$, accelerating the corrosion process (Li et al., 2016).

Only three corrosion models applied to slug pattern were found in the literature. They were both developed considering sweet corrosion in a horizontal pipeline. The first model, proposed by Jepson et al. (1996), employs the pressure gradient as the correlating parameter associating flow influence to CR. This model is based on Efird et al. (1993) work. The parameters of the empirical correlation were adjusted based on the experimental data. Thereafter, Nyborg et al. (2000) proposed a methodology for calculating the corrosion rate by splitting the slug flow into two parts: the liquid slug part and slug liquid film. The overall CR was then estimated by averaging the corrosion rates of these two zones, which were calculated assuming averaged wall shear stresses. At last, Wang et al. (2002) proposed a mechanist model using the same division method proposed by Nyborg et al. (2000). Two correlations were developed to determine a mass transfer coefficient in each zone. These mass transfer coefficients are used to evaluate the anodic/cathodic current densities and finally the CR. The predictions of Wang et al (2002) model are compared against the data provided by Jepson et al. (1997) exhibiting a tendency to overestimate the experimental data over 100% in certain cases.

Despite of the modeling efforts, these previous models are still limited to the conditions where they were developed. The aspects, which lead to a poor performance outside the scenarios where they were proposed, are still unclear. For Jepson et al. (1997) and Nyborg et al. (2000) models, one of the limiting factors might be the use of an average wall shear stress to estimate CR. Noticing that the average CR rising from the average wall shear stress is bias since the power function in Eq. (1) is not linear. The scenario is even worse if one considers the vertical slug flow where are found positive and negative $\tau_w$ values and the use of the average does not reflect the average of the positive nor of the negative values. Furthermore, for Jepson et al. (1997) model, the use of pressure gradient in vertical slug flow is even worse because the pressure drop is composed by two terms: the wall shear stress and the weight of the mixture being the last nearly 90% of the total pressure drop. Complementarily, Wang et al. (2002) model's problem is likely to be on the particular correlations for the mass transfer coefficients for each zone.

The objective of this work is to develop a methodology to estimate the wall shear stress as a form to assist future developments of corrosion models. The methodology is applied to upward vertical slug flows. The numerical estimate of the local wall shear stress discloses a not uniform $\tau_w$ profile along a slug unit. The $\tau_w$ data are provided for a range of gas-liquid velocities in a dimensionless form allowing a general use as a form to overcome the so-called two-phase flow effects on the corrosion models as far as the wall shear stress is concerned.

## 2. PROBLEM FORMULATION

The vertical upward slug flow is characterized by a quasi-periodic occurrence of aerated liquid slugs trailed by elongated bubbles, named as Taylor bubble. The Taylor bubble, surrounded by a liquid film, has a bullet-shaped format with round nose, nearly flat rear, and occupies almost all cross-sectional area of the tube. As the Taylor bubble displaces upward the thin liquid film moves downward. At the liquid slug the gas and the liquid flow with an upward direction. Wallis (1969) introduced the concept of unit cell approaching the flow as periodic with repeating cells consisting of a liquid slug trailed by an elongated bubble as a way to simplify the phenomena. These repeating cell are called as unit cells. Figure 1 shows: a schematic representation of a unit cell; the variables associated for a non-aerated liquid slug; the streamlines for a fixed frame of reference and a schematic wall shear stress distribution. The lengths of Taylor bubble and liquid slug are, respectively, $L_S$ and $L_f$; $u_t$ is the translational velocity of bubble's nose, $u_f$ is the velocity of falling liquid film around Taylor bubble and $u_{LS}$ is the velocity of the liquid phase on the liquid slug; $R_S$ and $R_f$ are the liquid holdup on the liquid slug and on the liquid film surrounding the Taylor bubble, respectively. The right side of Figure 1 displays a schematic representation of the wall shear stress along a unit cell. If the flow near the pipe wall is on upward or downward directions, the wall shear stress is negative or positive, respectively.

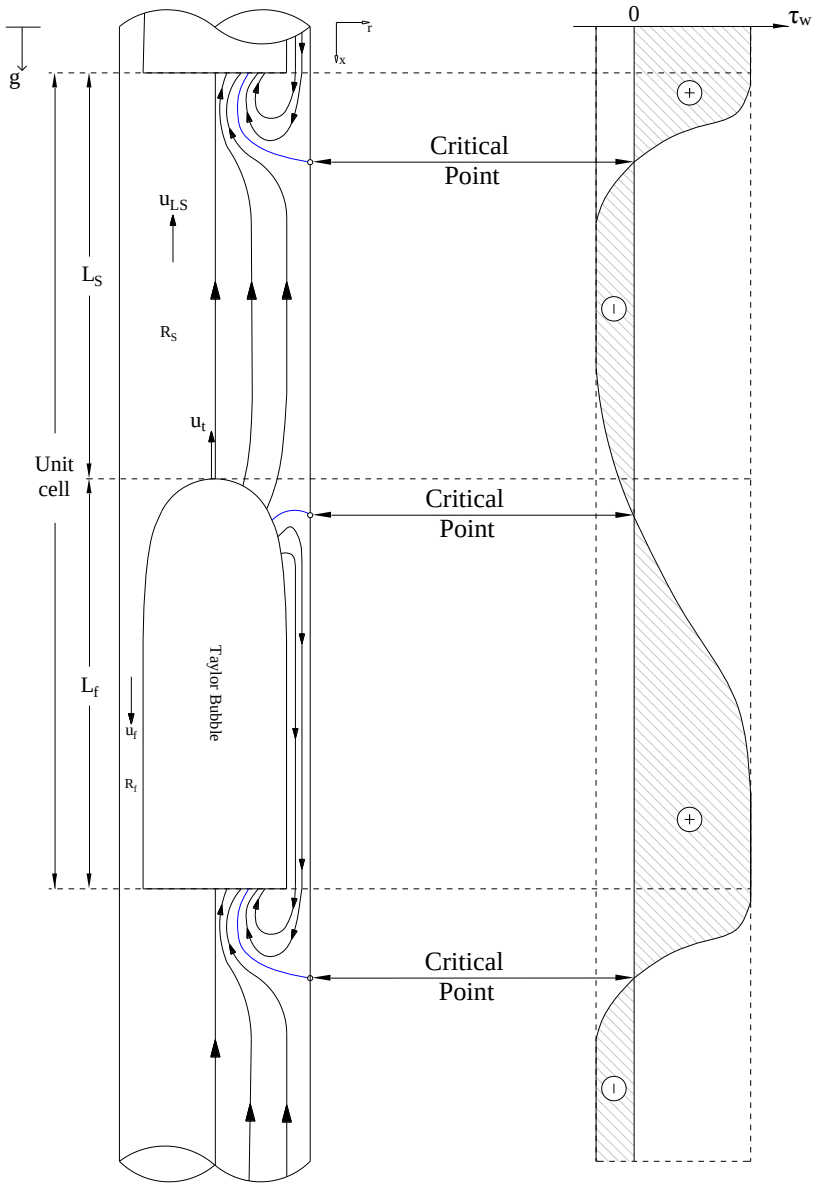


Figure 1. Unit cell with streamlines for a fixed frame of reference and the main flow parameters. At left a schematic representation of the wall shear stress.

The alternating passage of liquid slugs and liquid film shifts the flow direction between upward and downward, resulting in a wall shear stress value with negative and positive signs, respectively. At least, this evidence is shown in nine experimental works which used electrochemical method for measuring wall shear stress in a vertical slug flow: Cognet et al. (1984); Nakoryakov et al. (1986, 1989); Mao and Dukler (1989); Yan and Che (2011); Zheng and Che (2006) and Yan et al. (2012). At the transition between positive and negative wall shear stress there is a point where the wall shear stress is null. These points are called critical points because the velocity and the shear stress are zero. Furthermore, near a critical point, the wall shear stress is not uniform but it is constantly changing due to the change of +/- signal. Therefore, it might be expected, at least near a critical point the hypothesis of uniform wall shear stress will fail.

The influence of the critical points is better appraised through the schematic representation of the streamlines and wall shear stress distribution for a stationary frame of reference, Fig. 1. The upward displacement of the Taylor bubble dislodges a certain volume of fluid. Part of displaced volume flows upward while the other part flows downward forming the liquid film. The critical point at the bubble nose region is defined by the point of attachment of the dividing streamline that separates the flow in upward and downward directions, see representation on the figure (blue line). The liquid film develops downward, accelerating by gravity force, which is counter balanced by the ever changing wall shear stress. Eventually, if the film has enough length, it reaches equilibrium having the film thickness and the wall shear stress constants. The liquid film is discharged at the Taylor bubble rear in a form of a water jet into the upward liquid

slug. This liquid jet has momentum to penetrate at certain distance on the upward liquid slug until decelerate to zero velocity, forming the stagnation point near the bubble rear, see streamlines pattern on the figure.

## 3. WALL SHEAR STRESS MODELLING FOR UPWARD VERTICAL SLUG FLOW

The used fluids for estimating the wall shear stress profile are air ($\rho_G$ = 1.29 kg/m$^3$ and $\mu_G = 1.74 \cdot 10^{-5}$ Pa.s) and water ($\rho_L$ = 999 kg/m$^3$ and $\mu_L = 1 \cdot 10^{-3}$ Pa.s). Figure 2 shows the operational conditions on the vertical flow map proposed by Taitel et al. (1980). The x and y axes of the figure display the gas and liquid superficial velocities defined as:

$$J_G = \frac{Q_G}{A} \quad and \quad J_L = \frac{Q_L}{A} \tag{3}$$

where Q is the *in situ* volumetric flow rate, the subscripts $_G$ and $_L$ stand for gas or liquid phase and A is the pipe cross section area. The studies are carried out in a slug unit for tubes with internal diameter, ID, of 0.050, 0.075 and 0.100 m and superficial mixture velocities J defined as:

$$J = J_G + J_L \tag{4}$$

which has assumed the values of 1, 2 and 3 m/s.

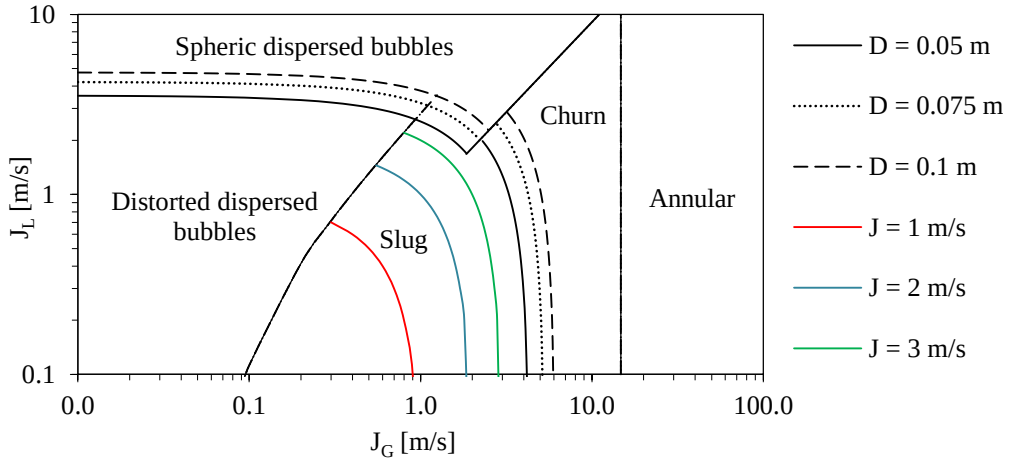


Figure 2.Vertical flow map by Taitel et al. (1980)

The wall shear stress data, despite being generated using water-air mixture, can be generalized to distinct fluid properties and operational conditions as long as the flow regimes on the liquid slug and liquid film are turbulent. For generalization purposes, the liquid slug is considered not aerated. This assumption reduces the dependence of the operational conditions of $J_G$ and $J_L$ to only J. In fact, for non-aerated liquid slug the liquid phase velocity is coincident the J. Complementarily, the liquid film model will demand the liquid slug velocity and the Taylor bubble velocities, which are also dependent of J. Therefore, to define the wall shear stress the required operational condition is only the mixture velocity. For convenience, J is also represented on Figure 2 disclosing that a large area of the slug flow occurrence on the map is covered by the chosen set of velocities.

### 3.1 Wall shear stress model at the liquid slug

The wall shear stress distribution in the liquid slug region is estimated through numerical simulation using Phoenics® (2011). With a frame of reference attached to the rising Taylor bubble the simulations are carried out in steady state. At this frame of reference, the Taylor bubble becomes stationary and the tube's wall moves downwards with velocity $u_t$. The domain length is 16D, which is enough for reaching a hydrodynamic developed flow in the liquid slug (Moissis and Griffith, 1962; Taitel et al., 1980). The *k-e* Chen and Kim (1987) model is used for simulating the liquid slug turbulent liquid flow. In addition, a special care was taken to locate the first grid nodes in the logarithmic law region, $40 < y^+ < 300$.

Figure 3 displays the computational domain as well as the boundary conditions. The frame of reference is positioned at the pipe centerline being x the axial coordinate aligned with the gravity acceleration and r the radial coordinate. The inlet is positioned at x = 0. The inlet axial velocity is $u_f + u_t$ corresponding to the width of a liquid film in equilibrium $h_{fe}$. To simulate the discharge of the liquid film into domain as water jet, is inserted a block of cells allowing slippage condition and length of 0.5D to simulate the Taylor bubble rear. The no-slip condition is applied to the pipe wall. The

wall velocity is equal to $u_t$. The outlet is positioned at 16D downstream the inlet and has a constant pressure. For reference, the parameters J, $u_f$, $u_t$ and $h_{fe}$ are displayed in Tab.1. The Reynolds number in the liquid slug region, ($Re_{LS}$), is calculated based on tube diameter and the mixture velocity. The liquid slug Re values range between a minimum of $5 \cdot 10^4$ with J = 1 m/s and D = 0.05 m and a maximum of $3 \cdot 10^5$, for J = 3 m/s and D = 0.100 m.

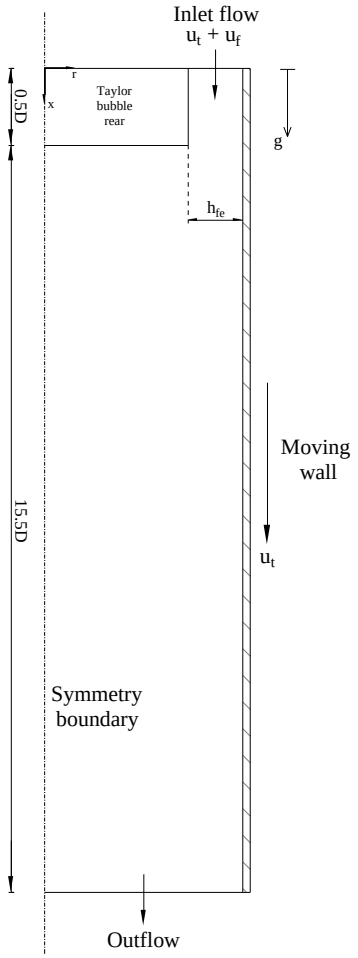


Figure 3. Computational domain and boundary conditions

Table 1. Input parameters

| D (m) | J (m/s) | $u_t$ (m/s) | $u_f$ (m/s) | $h_{fe}$ ($10^{-3}$ m) |
|---|---|---|---|---|
| 0.050 | 1 | 1.45 | 2.02 | 1.65 |
| | 2 | 2.65 | 2.08 | 1.76 |
| | 3 | 3.85 | 2.10 | 1.84 |
| 0.075 | 1 | 1.50 | 2.60 | 2.34 |
| | 2 | 2.70 | 2.69 | 2.50 |
| | 3 | 3.90 | 2.74 | 2.62 |
| 0.1 | 1 | 1.55 | 3.11 | 3.00 |
| | 2 | 2.75 | 3.23 | 3.21 |
| | 3 | 3.95 | 3.29 | 3.37 |

### 3.2 Wall shear stress model at the liquid film

The wall shear stress distribution along the liquid film is estimated using the one-dimensional film model proposed by Taitel and Barnea (1990). The model provides information about the thickness profile of the liquid film, the liquid holdup, film velocity and wall shear stress, along the axial coordinate. For negligible surface tension effect, the liquid and the gas phase share the same pressure. Using the momentum equation for the liquid and gas phase to eliminate the pressure dependence one gets the film equation as show in Eq. (5) for vertical flow with no aerated liquid slug.

$$\frac{dh_f}{dx} = -\frac{\dfrac{\tau_w S}{A_f} - \tau_i S_i \left( \dfrac{1}{A_f} + \dfrac{1}{A_G} \right) + \left( \rho_L - \rho_G \right) g}{\rho_L v_f \dfrac{\left( u_t - J \right)}{R_f^2} \dfrac{dR_f}{dh_f}} \tag{5}$$

where, the wall and the liquid film-gas shear stresses are $\tau_w$ and $\tau_i$; the liquid film – gas interface inner perimeter, $S_i$; film annular area, $A_f$; the gas area, $A_G$; the bubble nose translational velocity and mixture velocity, $u_t$ and J; relative film velocity for a frame of reference moving with the bubble nose velocity, $v_f$; film holdup, $R_f$; liquid and gas densities, $\rho_L$ and $\rho_G$; and gravity acceleration, g.

The geometrical relations for a vertical tube with a concentric interface are displayed in Tab.2. It is noted that all geometrical properties can be expressed as a function of the film thickness where D is the inner pipe diameter.

Table 2. Geometrical relations for vertical and concentric interface

| | |
|---|---|
| $A_f$ | $\pi D^2(h_f/D)[1 - (h_f/D)]$ |
| $A_G$ | $[(\pi D^2)/4][1 - (2h_f/D)]^2$ |
| $S_f$ | $\pi D$ |
| $S_i$ | $\pi D[1 - (2h_f/D)]$ |
| $R_f$ | $4(h_f/D)[1 - (h_f/D)]$ |

The liquid film velocity, $u_f$, required for calculating parameters such as the wall shear stress, is obtained through a mass balance between the liquid film and liquid slug, Eq. (6). In addition, the relative film liquid velocity in respect to a frame of reference moving with bubble's nose velocity, $v_f$, is equal to $u_t$ minus $u_f$.

$$u_f = u_t + \frac{(J - u_t)}{R_f} \tag{6}$$

where $u_t$ is calculated based on the correlation proposed by Bendiksen (1984), Eq. (7), which expresses the translational velocity of the bubble's nose as a linear combination of the mixture velocity and the rising velocity of the elongated bubble in stagnant liquid, or, drift velocity. The two coefficients $C_0$ and $C_\infty$, are the distribution and drift parameters, with values of 1.2 and 0.345, respectively. These values are valid for turbulent regime and low viscosity liquids.

$$u_t = C_0 J + C_\infty \sqrt{gD} \tag{7}$$

At last, the wall shear stress is estimated using the absolute film liquid velocity, Eq. (8), with the corresponding Fanning friction factor, $f_f$, obtained from the Blasius correlation.

$$\tau_w = f_f \frac{\rho_L u_f |u_f|}{2} \quad where \quad f_f = \frac{0.079}{Re^{1/4}} \tag{8}$$

The rate of the liquid film thickness, $dh_f/dx$, with the distance from the nose, x, is integrated in conjunction with the mass balance equation, geometrical relations, shear stress relations and the Taylor bubble nose's velocity correlation. It was used the software Mathematica 9.0 to numerically integrate Eq. (5) as well as to create an algorithm to simultaneously solve it with the required auxiliary equations.

## 4. RESULTS AND DISCUSSIONS

The local wall shear stress properties: magnitude, signal and its distribution along the slug unit are shown in this section. Before presenting the wall shear stress data the next two sections supply the main characteristics of the liquid slug and of the liquid film properties such as the axial distance of the critical point, the maximum wall shear stress and the axial length necessary to achieve a liquid film in equilibrium.

### 4.1 The liquid slug

The axial position of the critical point at the liquid slug is evaluated through the CFD analysis. The dimensionless distance from the Taylor bubble rear, $L_{crit1}/D$, is shown in Tab.3. As observed, the data do not show a significant difference among all cases studied but ranges between 3.53 to 5.42 pipe diameters downstream the Taylor bubble rear.

Upstream the liquid slug critical point the flow eventually becomes fully developed reaching its maximum wall shear stress in absolute value. For reference, these values are shown in Tab.4 in Pa. They were estimated using Colebrook correlation for smooth wall pipes and the mixture velocity, J. It is noted that the reference wall shear stress has a small change along the pipe diameter but changes with the mixture velocity nearly proportional to the square of the mixture velocity.

Table 3. Dimensionless axial distance of the liquid slug critical point, $L_{crit1}$ /D

| J (m/s) \ D (m) | 0.050 | 0.075 | 0.100 |
|---|---|---|---|
| 1 | 4.2 | 5.1 | 5.4 |
| 2 | 3.8 | 4.6 | 5.3 |
| 3 | 3.5 | 4.3 | 5.1 |

Table 4. Liquid slug absolute maximum wall shear stress (Pa)

| J (m/s) \ D (m) | 0.050 | 0.075 | 0.100 |
|---|---|---|---|
| 1 | 2.61 | 2.39 | 2.25 |
| 2 | 8.99 | 8.27 | 7.81 |
| 3 | 18.61 | 17.18 | 16.26 |

### 4.2 The liquid film

The dimensionless axial distance of the critical point below the bubble nose is displayed in Tab.5. The minimum distance was 1.0D for J = 1 m/s and D = 0.100 m, whereas the maximum was of 13.0D for J = 3 m/s and D = 0.050 m.

Table 5. Dimensionless axial distance of the critical point, $L_{crit2}$ /D, below the bubble nose.

| J (m/s) \ D (m) | 0.050 | 0.075 | 0.100 |
|---|---|---|---|
| 1 | 1.9 | 1.3 | 1.0 |
| 2 | 6.9 | 4.5 | 3.5 |
| 3 | 13.0 | 9.2 | 7.1 |

The flow is on the upward direction in the region comprised between the Taylor bubble's nose up to the critical point. The wall shear stress is negative but increase steadily until the critical point is reached and the stress is null. Downstream the critical point the flow is on the downward direction, the wall shear stress is positive and the flow is accelerated by gravity. If the liquid film has enough length eventually, the equilibrium is reached and the film weight is balanced by the wall shear stress.

At the film equilibrium condition, the shear stress reaches a maximum value. The maximum film wall shear stress' value is shown on Tab.6 in Pa as a function of pipe diameter and mixture velocity. The wall shear stress values spanned from 15.14 Pa to J = 1 m/s and D = 0.050 m up to 29.76 Pa for J = 3 m/s and D = 0.100 m. For reference, Tab.7 shows the dimensionless film length necessary to achieve the equilibrium condition. Keeping the mixture velocity constant the film developing length decreases as the pipe diameter increases. Complementarily, fixing a pipe diameter the film length increases proportionally to the mixture velocity. The change on the film length to achieve the equilibrium condition is more sensitive to the mixture velocity rather than to the pipe diameter.

Table 6. Liquid film maximum wall shear stress (Pa)

| J (m/s) \ D (m) | 0.050 | 0.075 | 0.100 |
|---|---|---|---|
| 1 | 15.14 | 21.57 | 27.73 |
| 2 | 15.70 | 22.54 | 29.07 |
| 3 | 15.80 | 23.00 | 29.76 |

Table 7. Dimensionless liquid film equilibrium length , $x_{eq}$ /D

| J (m/s) \ D (m) | 0.050 | 0.075 | 0.100 |
|---|---|---|---|
| 1 | 25.3 | 24.7 | 24.5 |
| 2 | 39.9 | 36.7 | 35.3 |
| 3 | 54.1 | 49.3 | 46.1 |

### 4.3 Wall shear stress distribution in a slug unit

The dimensionless wall shear stress distributions over a slug unit, for mixture velocities of 1, 2 and 3 m/s at pipe diameters of 0.050, 0.075 and 0.100 m ID, are displayed in Fig.4 in conjunction with a schematic representation of a liquid slug trailed by a Taylor bubble on the figure's left side. This schematic representation was inserted to assist the graphics interpretation. It was used two distinct normalizing scales for the wall shear stress, $\tau_{ref}$: One for the positive and another for the negative values of wall shear stresses. The scales for positive and negative wall shear stresses are, respectively, the liquid film wall shear stress at the equilibrium condition and the liquid slug wall shear stress at fully developed state. For referencing purposes, the magnitudes of these scaling values are shown in Tab.4 and Tab.6, respectively. The convenience of using two scales for the wall shear stress is to bound the dimensionless wall shear values to -1 to +1 which allows an easy comparison among distinct curves. The x-axis corresponds to the liquid slug length trailed by the liquid film length. The x scale is at the right of the figure and represents the lengths of the liquid slug and the liquid film expressed in pipe diameters. The liquid slug length is limited to 16D, a necessary length to get fully developed state. At axial distances beyond 16D it is considered that the wall shear stress is no longer changing and, therefore, an extrapolation can be made just using the wall shear stress corresponding to the fully developed state. The

three consecutive dots between the liquid slug and liquid film graphs represent the liquid slug fully developed region. The liquid film starts at the bubble nose, where x = 0 and the axial scale goes up to 60D, the necessary liquid film length to get the equilibrium state. Liquid films lengthier than 60D have the wall shear stress constant and equal to the one found on the equilibrium state.

A visual inspection on Fig.4 discloses that the liquid slug dimensionless wall shear stress is close to +1 at the bubble rear and decreases toward zero as the distance increases. This region corresponds to the deceleration of the liquid film jet near the wall and finishes at the liquid slug critical point. Beyond this critical point, the flow develops to reach the fully developed state where the dimensionless shear stress is -1. The liquid film dimensionless wall shear stress starts at the bubble nose sharing the same negative value of the liquid slug, i.e. -1. As the liquid film develops, it reaches the critical point where the wall shear stress is null. Beyond the critical point, the dimensionless wall shear stress is positive and increases up to the maximum value corresponding to a liquid film in equilibrium, i.e. +1.

It is observed, placing together the liquid slug and film wall shear stress distributions that they show periodic behavior due the usage of unit cell concept. The regions with the largest changes on the dimensionless wall shear stress are the ones related to the critical points both in the liquid slug and in the liquid film; more specifically, where the dimensionless wall shear stress crosses the line corresponding to zero along the y-axis.

The outcome of the dimensionless wall shear stresses at the liquid slug is almost similar as far as the mixture velocity and pipe diameter changes. However, the dimensionless wall shear stress at the liquid film is discriminated by the mixture velocity.

The data shown in Fig.4 allows one to develop a corrosion model taking into account the local wall shear stress values changing periodically in space or time. The residence time is derived by simply taking the ratio $L_f/u_t$ and $L_S/u_t$. The information in Tab.4 and Tab.6 disclose the maximum wall shear stress at the liquid slug is sensitive to the mixture velocity, J, but at the liquid film, it is sensitive to the pipe diameter. Therefore, the reference values to the liquid slug and liquid film changes distinctly if the mixture velocity or the pipe diameter changes. Furthermore, the lengths or the time intervals of the reference values also changes due to the phases flow rates.

The data presented in Fig. 4 can be used for liquid slug longer than 16D and liquid film longer than 60D just using the wall shear stresses for fully developed state and equilibrium state respectively. On the contrary, if the liquid slug and the film length were shorter than 16D and 60D then they will not reach fully developed state neither equilibrium state and the cycle will be bounded by values of $|\tau_w/\tau_{res}| < 1$ which can be evaluated on the figure accordingly to the average length of the liquid slug and liquid film.

## 5. CONCLUSION

The major contribution of this work is the disclosure of the non-uniformity of the wall shear stress distributions overlooked on previous corrosion models. The periodic wall shear stresses disclose in a concise form that CR depend on the local wall shear stress as well as on the lengths, or residence time, of the liquid slug and liquid film. The development of new CR models have necessarily to embody the two-phase flow effects of the slug flow considering the local wall shear stress and the lengths of the liquid slug and liquid film.

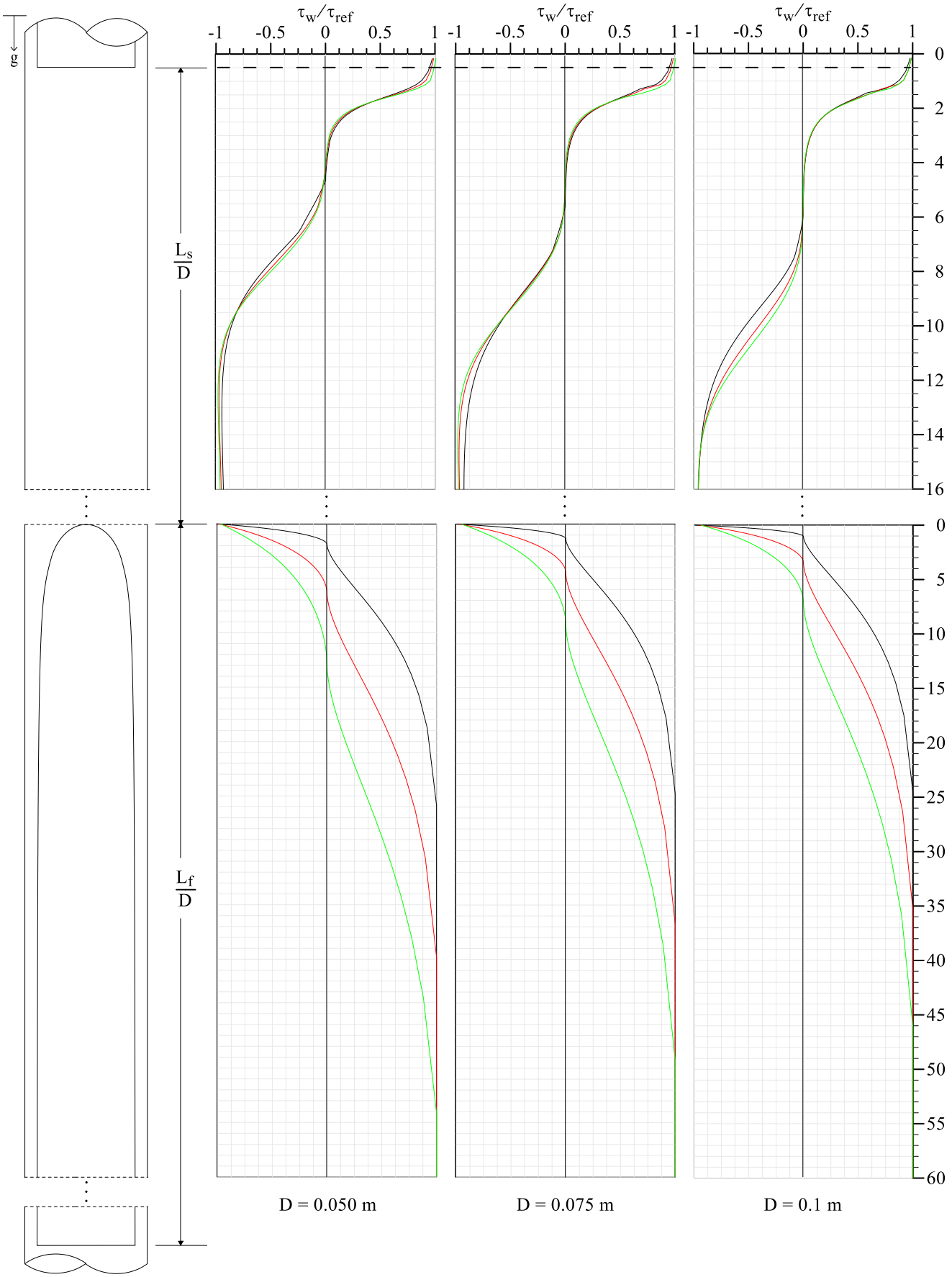


Figure 4. Dimensionless wall shear stress profile in a slug unit; —— J = 1 m/s; —— J = 2 m/s; —— J = 3 m/s.

## 5. ACKNOWLEDGEMENTS

The authors acknowledge the financial support from Petrobras

## 6. REFERENCES

Bendiksen, K. H., 1984. "An experimental investigation of the motion of long bubbles in inclined tubes". International Journal of Multiphase Flow, Vol.10, No. 4, pp. 467–483.

Cognet, G., Lebouche, M., Souhar, M., 1984. "Wall shear measurements by electrochemical probe for gas-liquid two-phase flow in vertical duct". AIChE Journal, Vol. 30, No. 2, pp. 338-341.

Chen, Y.S. and Kim, S. W., 1987. "Computation of turbulent flows using an extended k-e turbulence closure model", NASA CR-179204.

Efird, K. D., Wright, E. J., Boros, J. A., & Hailey, T. G., 1993. "Wall shear stress and flow accelerated corrosion of carbon Steel in Sweet Production". International Corrosion Congress, Vol. 14, p. 194.

Gopal, M., Kaul, A., Jepson, W.P., 1995. "Mechanisms contributing to enhanced corrosion in three phase slug flow in horizontal pipes". Corrosion/95. NACE International, Paper No. 105.

Green, A. S., Jonhnson, B. V., Choi, H., 1990. "Flow-related corrosion in large diameter multiphase flow line". Society of Petroleum Engineers. SPE 20685

Jepson, W. P., Bhongale, S., Gopal, M., 1996. "Predictive model for sweet corrosion in horizontal multiphase slug flow". Corrosion/96. NACE International, paper no. 19.

Kanwar, S. and Jepson, W. P., 1994. "A model to predict sweet corrosion of multiphase flow in horizontal pipelines". Corrosion/94. NACE International, Paper No. 24.

Li, W., Pots, B. F. M., Brown, B., Kee, K. E., Neisic, S., 2016. "A direct measurement of wall shear stress in multiphase flow – Is it an important parameter in $CO_2$ corrosion of carbon steel pipelines?". Corrosion Science.

Mao, Z. S. and Dukler, A. E., 1989. "An experimental study of gas-liquid slug flow". Experiments in Fluids, Vol. 8, No. 3-4, pp. 169-182.

Moissis, R. and Griffith, P., 1962. "Entrance effects in a two-phase slug flow".Journal of Heat Transfer, Vol. 84, No. 1, pp. 29-38.

Nakoryakov, V. E., Kashinsky, O. N., Kozmenko, B. K., 198. "Experimental study of gas-liquid slug flow in a small-diameter vertical pipe". International Journal of Multiphase Flow, Vol 12, No. 3, pp. 337-355.

Nakoryakov, V. E., Kashinsky, O. N., Petukhov, A. V., Gorelik, R. S., 1989. "Study of local hydrodynamic characteristics of upward slug flow". Experiments in Fluids, Vol. 7, No. 8, pp. 560-566.

Nicklin, D. J., Wilkes, J. O., Davidson, J. F., 1962. "Two-phase flow in vertical tubes". Transactions of the Instution of Chemical Engineers, Vol. 40, No. 1, pp. 61-68.

Nyborg, R., Andersson, P., Nordsveen, M., 2000. "Implementation of $CO_2$ corrosion models in a three-phase fluid flow model". Corrosion/2000. NACE International, Paper No. 48.

Shoham, O., 2006. Mechanistic modeling of gas-liquid two-phase flow in pipes. Richardson, TX: Society of Petroleum Engineers.

Sun, J. Y. and Jepson, W. P., 1992. "Slug flow characteristics and their effect on corrosion rates in horizontal oil and gas pipelines". Society of Petroleum Engineers. SPE 24787.

Taitel, Y. and Barnea, D., 1990. "Two-phase slug flow". Adv. Heat Transfer, Vol. 20, pp. 83-132.

Taitel, Y., Bornea, D., Dukler, A. E., 1980. "Modelling flow pattern transitions for steady upward gas-liquid flow in vertical tubes". AIChE Journal, Vol. 26, No. 3, pp. 345-354.

Wang, H., Cai, J. Y., Jepson, W. P. 2002. "CO2 corrosion mechanistic modeling and prediction in horizontal slug flow". Corrosion/2002. NACE International, Paper No. 02238.

Wallis, G.B., 1969. One-dimensional two-phase flow. New York: McGraw-Hil.

Yan, K. and Che, D., 2011. "Hydrodynamic and mass transfer characteristics of slug flow in a vertical pipe with and without dispersed small bubbles". International Journal of Multiphase Flow, Vol. 37, No. 4, pp. 299-325.

Yan, K., Zhang, Y., Che, D., 2012. "Experimental study on near wall transport characteristics of slug flow in a vertical pipe". Heat and Mass Transfer, Vol. 48, No. 7, pp 1193-1205.

Zheng, D. and Che, D., 2006. "Experimental study on hydrodynamic characteristics of upward gas–liquid slug flow". International Journal of Multiphase Flow, Vol. 32, No. 10, pp. 1191-1218.

Zhou, X., 1993. Experimental study of corrosion rate and slug flow characteristics in horizontal, multiphase pipeline. PhD thesis, Ohio University, Athens, OH, USA.

## 7. RESPONSIBILITY NOTICE

The authors are the only responsible for the printed material included in this paper.